Colloids and Surfaces B: Biointerfaces 218 (2022) 112716

Contents lists available at ScienceDirect

Colloids and Surfaces B: Biointerfaces

journal homepage: www.elsevier.com/locate/colsurfb

Single-particle detection of native SARS-CoV-2 virions by microfluidic resistive pulse sensing

Zoltán Varga [a,*], Mónika Madai [b], Gábor Kemenesi [b], Tamás Beke-Somfai [a], Ferenc Jakab [b]

[a] Biological Nanochemistry Research Group, Institute of Materials and Environmental Chemistry, Research Centre for Natural Sciences, Magyar Tudósok Körútja 2, H-1117 Budapest, Hungary
[b] National Laboratory of Virology, Szentágothai Research Centre, University of Pécs, Ifjúság Útja 20, H-7624 Pécs, Hungary

ARTICLE INFO

Keywords:
SARS-CoV-2
Viral envelope
Size distribution
Resistive pulse sensing
Spike protein

ABSTRACT

Microfluidic resistive pulse sensing (MRPS) was used to determine the size –distribution of severe acute respiratory syndrome coronavirus 2 (SARS-CoV-2) based on detecting nearly 30,000 single virions. However, the ultrastructure of SARS-CoV-2 is thoroughly described, but ensemble properties of SARS-CoV-2, e.g., its particle size distribution, are sparsely reported. According to the MRPS results, the size distribution of SARS-CoV-2 follows a log-normal function with a mean value of 85.1 nm, which corresponds to an approximate diameter of the viral envelope. This result also confirms the low number (< 50) of spike proteins on the surface of the virions.

1. Introduction

The ongoing coronavirus disease 2019 (COVID-19) pandemic caused by the severe acute respiratory syndrome coronavirus 2 (SARS-CoV-2) enormously challenged the world. Although the scientific efforts brought us closer to the possibility of keeping the pandemic on a controlled track, the appearance of new variants indicates that pandemics will stay with us for extended periods. Thus, it is vital to expand our knowledge about SARS-CoV-2.

Clinically approved diagnosis of COVID-19 is either based on the detection of the viral ribonucleic acid (RNA) with real-time reverse transcription polymerase chain reaction (RT-PCR) [1] or the detection of viral proteins with specific antigen tests utilizing lateral flow immunoassay (LFIA) [2]. Besides, novel methods using, for example, total internal reflection ellipsometry [3], electrochemical impedance spectroscopy [4], or molecularly imprinted polymers [5] were also reported to detect SARS-CoV-2.

Structural properties of the virus have been extensively studied since the pandemic's beginning. Thanks to novel methods, such as cryo-electron tomography, the ultrastructure of SARS-CoV-2 is thoroughly described [6–9]. However, studies that aim to determine ensemble properties of the virions, e.g., their particle size distribution, are lacking. Since the size of a SARS-CoV-2 virion is in the 100 nm range, nanoparticle measurement methods, such as dynamic light scattering (DLS) [10,11] nanoparticle tracking analysis (NTA) [12,13] and resistive pulse sensing (RPS) [14], are theoretically suitable for its characterization. However, methods based on light scattering could overestimate the size of the virions due to the strong dependence of the intensity of the scattered light on the particle diameter.

On the other hand, detection of particles by nanopore-based RPS is feasible independently of the particles' refractive index, enabling the use of reference nanoparticle standards to characterize biological soft colloids, such as virus particles. Reference materials certified by metrology institutes are commonly made of gold, silica, and polystyrene, which can be used for optical methods only if the refractive index of the measurand nanoparticles matches that of the reference material.

Microfluidic RPS (MRPS) is a novel nanoparticle characterization method that can provide size and concentration measurements on a statistically relevant number of particles due to its high particle detection rate (approx. 10,000 particles/s) with the precision of single-particle counting methods [15]. Detection of nanoparticles using MRPS is based on the Coulter principle, i.e., particles suspended in an electrolyte solution pass through a constriction, resulting in a resistive pulse due to the displacement of the ions by the particle in the constriction. Pulse height is proportional to the volume excluded by the particle, while the frequency of the pulses in the knowledge of the flow rate can be used to determine the concentration.

In this study, we applied MRPS for the first time to detect intact

* Corresponding author.
E-mail address: varga.zoltan@ttk.hu (Z. Varga).

https://doi.org/10.1016/j.colsurfb.2022.112716
Received 24 March 2022; Received in revised form 8 July 2022; Accepted 21 July 2022
Available online 22 July 2022

SARS-CoV-2 virions and constructed its size distribution by counting nearly 30,000 individual particles.

2. Materials and methods

2.1. Sample preparation

Vero E6 (African green monkey kidney epithelial) cells (ATCC CRL-1586) were grown in T75 cell culture flasks at $5{\cdot}10^6$ cells/flask and used at approximately 90% confluence. The cells were infected with SARS-CoV-2 (hCoV-19/Hungary/SRC_isolate_2/2020, Accession ID: EPI_ISL_483637) at an MOI (multiplicity of infection) of 0.1.

After 30 min incubation in a humidified atmosphere of 5% CO_2 at 37 °C, the culture medium was removed and replaced with a fresh culture medium without serum. Forty-eight hours post-infection, the cytopathogenic effect was evaluated by microscopic observation, and the supernatants were collected. Removal of cells and debris was performed by centrifugation at 800 x g for 10 min. The remaining debris was removed by filtration using a 0.45 μm syringe filter. The filtered cell-free supernatant was concentrated 10-fold by tangential flow filtration using a TFF-Easy (HansaBioMed, Tallin, Estonia) device. The control sample without infection was prepared using the same conditions and procedures.

2.2. Microfluidic resistive pulse sensing measurements

MRPS measurements were performed on an nCS1 instrument (Spectradyne LLC, Signal Hill, CA, USA). 90 μL concentrated cell-free supernatant was mixed with 10 μL bovine serum albumin (BSA, A2153, Sigma-Aldrich, Hungary) solution at 10 mg/mL in PBS buffer, filtered through a VivaSpin 500, 100 kDa MWCO membrane filter (Sartorius, Germany). The addition of the BSA solution is necessary to reduce the surface tension of the buffer to ensure the proper wetting of the microfluidic channels. Samples with a volume of 5 μL were measured using TS-400 cartridges, with a measurement range of 65–400 nm.

Traceable polystyrene (PS) bead with a 90 nm nominal diameter was used for calibration (PS90, 1 w/v%, Polysciences Inc.). The stock solution of the particle standard was diluted to 4000-fold in 1 mg/mL filtered BSA solution.

3. Results and discussion

3.1. Calibration with standard polystyrene nanoparticles

Fig. 1. shows the detection of NIST traceable polystyrene standard particles with a nominal diameter of 90 nm. The time course of the voltage signal (Fig. 1a) contains spikes, also termed pulses, which correspond to individual particles passing through the nanopore. The height of the pulses can be calibrated to diameter using nanoparticle standards with known diameter, and the size distribution of the particles can be obtained as a histogram of the individual peak data (Fig. 1b).

Since the microfluidic cartridge's maximum detection rate can reach 10,000 particles/seconds, a high-resolution size distribution can be obtained by counting a statistically significant number of particles. The single-use microfluidic cartridges of the nCS1 instrument are factory-calibrated, but here the PS90 measurement was used to post-calibrate the cartridge used to measure the virions. The calibration factor for the diameter was found to be 0.928. It should be emphasized that MRPS is a non-optical method hence the refractive index mismatch between PS and biological nanoparticles does not compromise the usability of PS nanoparticles as a reference standard in these measurements.

The concentration of the PS90 sample can be estimated based on the dry weight content and can be used to estimate the particle number concentration. However, as certified reference material is not available for particle number concentration of nanoparticles, the concentration value obtained by this method is not traceable. Moreover, the density of the particles and the dilution error also contribute to the uncertainty of this value. Using the values of 1 w/v% and 1.050 g/cm^3 for mass concentration of the PS90 sample and density of polystyrene, respectively, the nominal concentration of the standard sample was $6.25{\cdot}10^9$ mL^{-1}. In contrast, the measured concentration was found to be $2.79{\cdot}10^9$ mL^{-1}, which implies a calibration factor for the concentration of 2.24.

3.2. Size distribution of the cell-free supernatant without infection

The size distribution obtained for the control cell-free supernatant without infection is shown on a linear scale in Fig. 2a. A monotonically decreasing curve can be observed on the detection range of the used cartridge (65–400 nm), which can be attributed to extracellular vesicles (EVs) and other particles present in the culture medium. The size distribution is shown in Fig. 2b on a log-log plot. This representation emphasizes that particles above 100 nm are also present in the sample but at a much lower concentration than the sub 100 nm particles. The log-log plot is also helpful in investigating the shape of the distribution. It was proposed that the size distribution of EVs follows a power-law function [16], which is represented as a straight line on the log-log plot. The size distribution in the 100–200 nm range can be well described with a power-law function with an exponent of − 5.5, but a deviation from this trend is also apparent at the low end of the size distribution (from 65 nm to 100 nm). This observation can be explained by the heterogeneous composition of the cell-free supernatant. In summary, the size distribution of the control sample is a monotonically decaying distribution without any characteristic peaks.

3.3. Size distribution of the cell-free supernatant after infection

The size distribution of the cell-free supernatant of SARS-CoV-2 infected Vero cells are shown on a linear and a log-log scale in Fig. 2c

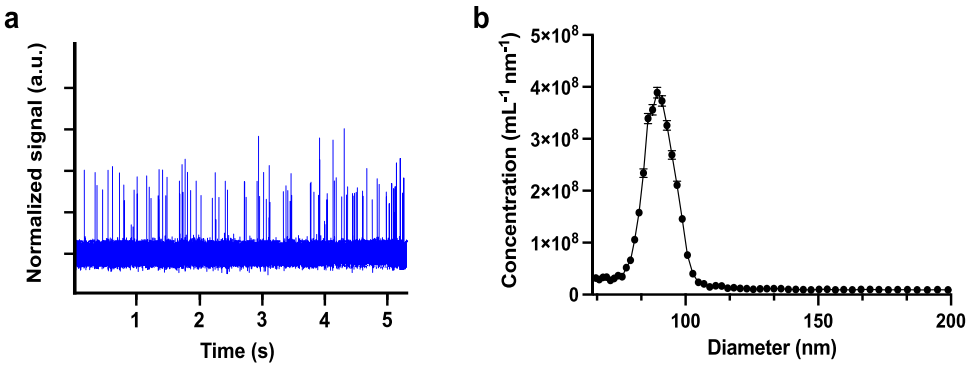

Fig. 1. Detection of standard polystyrene nanoparticles (nominal diameter of 90 nm) with MRPS. (a) Time course of the voltage signal exhibit pulses caused by individual particles passing through the nanoconstriction. (b) Concentration spectral density function.

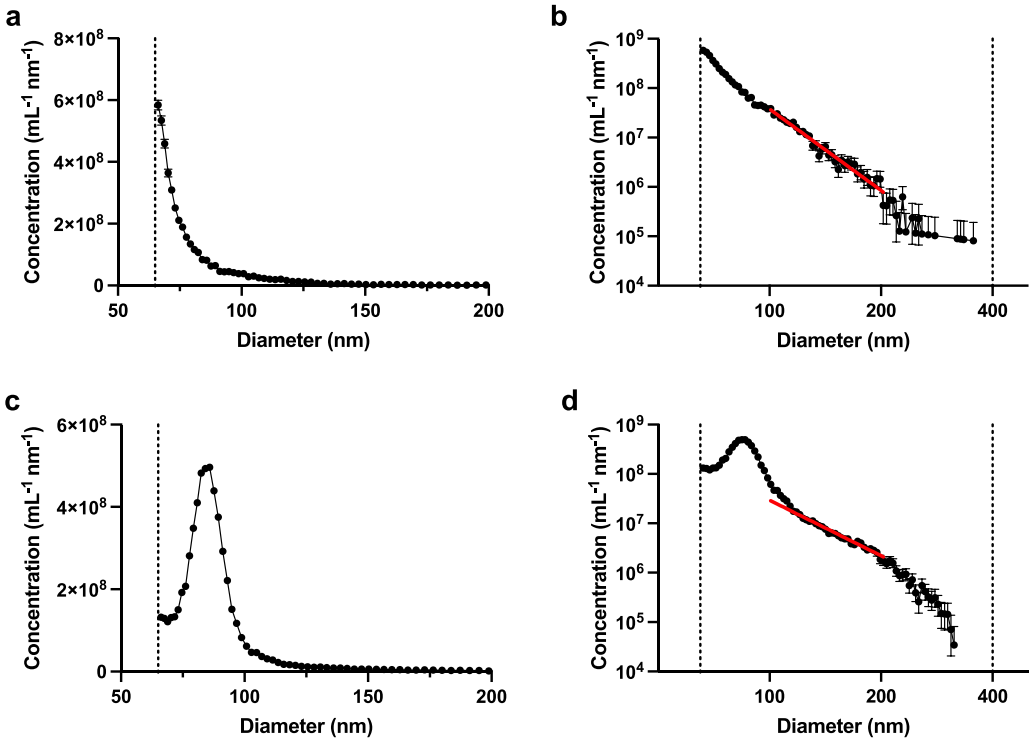

Fig. 2. Size distributions of the control cell-free supernatant without infection (a, b) and after SARS-CoV-2 infection (c, d). Panels a and c show the distributions on a linear scale, while panels b and d show the same distributions on a log-log plot. Dashed vertical lines indicate the size range limits of the used microfluidic cartridges, and solid red lines represent the best-fitting power-law functions on the 100–200 nm size range.

and d, respectively. The distribution was constructed from the detection of 49 366 individual particles. In contrast to the control sample, the measured size distribution of the cell-free supernatant of infected cells indicates a homogeneous particle size distribution with a peak around 90 nm diameter. Besides the characteristic peak of the virions, a background of a heterogeneous particle distribution can also be observed, which is best seen in the log-log representation. This background distribution resembles the one observed for the uninfected cell-free supernatant and can be well described with a power-law function with an exponent of − 3.7. MRPS measures the absolute concentration of the particles; hence direct subtraction of a background distribution is feasible in general. However, it cannot be carried out in the current case due to changes in the normal vesiculation of the cells because of the viral infection. Most probably, the enhanced cell death due to the infection is also responsible for the change in the exponent of the background. Though the quantitative comparison of the background particles in control and the infected samples is not feasible, it can be concluded that the infection does not cause a significant change in the overall vesicle or, more generally, in non-viral particle concentration. In interpreting the latter, of course, the decrease of the cell number due to infection must be considered.

3.4. *Quantitative analysis of the size distribution of SARS-CoV-2 virions*

For the quantitative analysis of the size distribution of the virions, first, the fitted background function was subtracted from the measured dataset. The original size distribution and the estimated background are shown in Fig. 3a, while Fig. 3b shows the background corrected data. Next, fitting of the measured data was attempted with peak functions of various forms, including Gaussian and log-normal functions. Best fit based on the adjusted R^2 and reduced χ^2 values was obtained with a log-normal function in the form of:

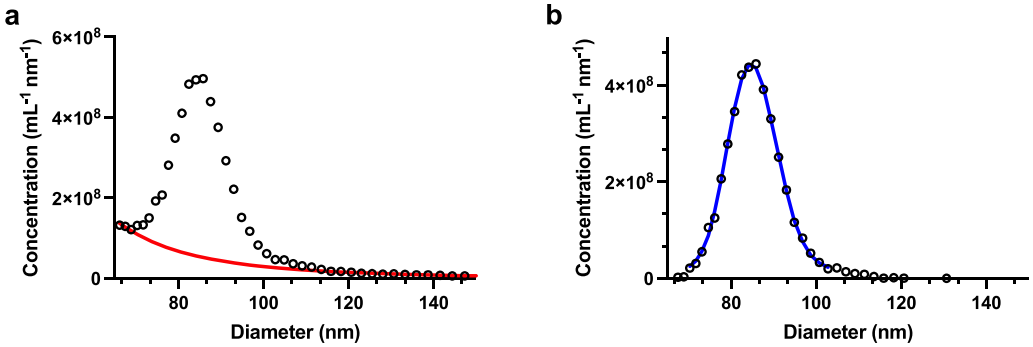

Fig. 3. Size distributions of native SARS-CoV-2 virions. (a) As measured distribution with the fitted power-law function to estimate the background of non-viral particles (solid red line). (b) Background corrected size distribution with the best fitting log-normal function. (For interpretation of the references to color in this figure legend, the reader is referred to the web version of this article.)

$$y = y_0 + \frac{A}{\sqrt{2\pi}wx} e^{-\frac{\left(\ln\frac{x}{x_C}\right)^2}{2w^2}},$$

where y_0 is the offset, x_C is the center, w is the log standard deviation, and A is the area of the distribution. From these parameters, the mean (μ) value can be calculated as:

$$\mu = e^{\ln(x_C)+w^2/2},$$

and the standard deviation (σ) as:

$$\sigma = e^{\ln(x_C)+w^2/2} \cdot \sqrt{e^{w^2} - 1}.$$

The fitted model function is also shown in Fig. 3b, while the best-fit parameters are summarized in Table S1 (Supplementary Materials).

The most important parameter of the distribution is the geometric mean which is the median in the case of the log-normal distribution. The 85.12 ± 0.06 nm value can be unrealistically small at first glance, considering the typical values reported in the literature for the size of SARS-CoV-2 virions [8]. To interpret the value obtained, the measuring principle of resistive pulse sensing should be considered. According to the Coulter principle, the observed resistive pulse is proportional to the volume excluded by the particle. In the case of solid nanoparticles, the diameter calculated from the excluded volume concurs with the volume determined by the physical boundary of the particle. However, these two values may differ significantly in the case of particles with inhomogeneous surface layers. Examples include particles with surface grafted macromolecules or with adsorbed protein corona [17]. In the case of SARS-CoV-2 virions, the phospholipid bilayer determines the envelope diameter.

In contrast, the outer diameter is given by the core diameter plus two times the thickness of the protein corona formed by the spike proteins on the surface of the virions. MRPS does not measure the outer diameter, but it provides a diameter value equivalent to a sphere with a volume of the core of the particles plus the total volume of the spike proteins on the surface. The difference between the envelope diameter and the diameter corresponding to the excluded volume can be estimated based on previous cryo-EM and AFM studies. Yao et al. used cryo-EM to investigate the ultrastructure of SARS-CoV-2 virions and obtained 80 nm for the average envelope diameter and 26 ± 15 for the number of spikes (S trimers) per virion [6]. Ke et al. found (91 ± 11) nm and 24 ± 9 for these values, also obtained by cryo-EM [8]. AFM investigations revealed (83 ± 7) nm for the height of antibody anchored virions and 61 spikes covering the virions on average, a value slightly higher than those obtained by electron microscopic observations [18]. The volume of a trimeric S protein is estimated to be 570 nm^3 based on its PDB structure (6VXX) [19] and using a voxel-based algorithm [20]. Using the average values for the structural parameters (i.e., 85 nm for the envelope diameter and 37 spikes per virion), one can theoretically obtain 86.8 nm for the diameter corresponding to the excluded volume, which means that MRPS practically measures the envelope diameter of the virions due to the low number of spike proteins on the surface of SARS-CoV-2 virions. Note that both the envelope diameter and the number of spikes per virion contribute to the apparent diameter measured by MRPS. Therefore, these values cannot be determined independently from MRPS only. Thus, the obtained values are in close agreement with previous observations, suggesting that the number of S trimers on the virion surface is relatively low compared to other enveloped viruses [6,18]. Also, suppose we add the 20–22.5 nm size of the spike protein for both sides of the virion to the obtained diameter value. In that case, we obtain approximately 125 nm for the virion's maximal outer diameter; a value frequently used to describe the dimensions of this novel coronavirus.

4. Conclusions

We have employed MRPS to determine the size distribution of SARS-CoV-2 virions based on counting a statistically significant ensemble of viral particles. Our results provide an average virion size of 85.12 nm ± 0.06 nm, which, based on the theoretical background of this method, also confirms that there are relatively few spike proteins on the surface of the virions. Moreover, MRPS provides a rapid particle number-based estimation of the viral concentration, which might be utilized in vaccine development in the future.

CRediT authorship contribution statement

Zoltán Varga: Conceptualization, Investigation, Formal analysis, Writing – original draft. **Mónika Madai:** Investigation. **Gábor Kemenesi:** Investigation. **Tamás Beke-Somfai:** Conceptualization, Investigation and Writing – original draft. **Ferenc Jakab:** Conceptualization, Writing – review & editing.

Declaration of Competing Interest

The authors declare that they have no known competing financial interests or personal relationships that could have appeared to influence the work reported in this paper.

Data availability

Data will be made available on request.

Acknowledgements

This work was funded by the National Research, Development and Innovation Office NKFIH, Hungary, under grant number 2020-1-1-2-PIACI-KFI_2020-00021. ZV was supported by the János Bolyai Research Scholarship of the Hungarian Academy of Sciences and by the New National Excellence Program of the Ministry for Innovation and Technology from the source of the National Research, Development, and Innovation Fund (ÚNKP-21-5 Bolyai+). TKP2021-NVA-07 and TKP2021- EGA-13 have been implemented with the support provided from the National Research, Development and Innovation Fund of Hungary, financed under the TKP2021-NVA and TKP2021-EGA funding scheme. This work was supported by the National Laboratory of Virology, project no. RRF-2.3.1-21-2022-00010.

Appendix A. Supporting information

Supplementary data associated with this article can be found in the online version at doi:10.1016/j.colsurfb.2022.112716.

References

[1] I. Smyrlaki, M. Ekman, A. Lentini, N. Rufino de Sousa, N. Papanicolaou, M. Vondracek, J. Aarum, H. Safari, S. Muradrasoli, A.G. Rothfuchs, J. Albert, B. Högberg, B. Reinius, Massive and rapid COVID-19 testing is feasible by extraction-free SARS-CoV-2 RT-PCR, Nat. Commun. 11 (2020) 4812, https://doi.org/10.1038/s41467-020-18611-5.

[2] Z. Li, Y. Yi, X. Luo, N. Xiong, Y. Liu, S. Li, R. Sun, Y. Wang, B. Hu, W. Chen, Y. Zhang, J. Wang, B. Huang, Y. Lin, J. Yang, W. Cai, X. Wang, J. Cheng, Z. Chen, K. Sun, W. Pan, Z. Zhan, L. Chen, F. Ye, Development and clinical application of a rapid IgM-IgG combined antibody test for SARS-CoV-2 infection diagnosis, J. Med. Virol. 92 (2020) 1518–1524, https://doi.org/10.1002/jmv.25727.

[3] I. Plikusiene, V. Maciulis, A. Ramanaviciene, Z. Balevicius, E. Buzavaite-Verteliene, E. Ciplys, R. Slibinskas, M. Simanavicius, A. Zvirbliene, A. Ramanavicius, Evaluation of kinetics and thermodynamics of interaction between immobilized SARS-CoV-2 nucleoprotein and specific antibodies by total internal reflection ellipsometry, J. Colloid Interface Sci. 594 (2021) 195–203, https://doi.org/10.1016/j.jcis.2021.02.100.

[4] V. Liustrovaite, M. Drobysh, A. Rucinskiene, A. Baradoke, A. Ramanaviciene, I. Plikusiene, U. Samukaite-Bubniene, R. Viter, C.-F. Chen, A. Ramanavicius, Towards an electrochemical immunosensor for the detection of antibodies against SARS-CoV-2 spike protein, J. Electrochem. Soc. 169 (2022), 037523, https://doi.org/10.1149/1945-7111/ac5d91.

[5] V. Ratautaite, R. Boguzaite, E. Brazys, A. Ramanaviciene, E. Ciplys, M. Juozapaitis, R. Slibinskas, M. Bechelany, A. Ramanavicius, Molecularly imprinted polypyrrole

based sensor for the detection of SARS-CoV-2 spike glycoprotein, Electrochim. Acta 403 (2022), 139581, https://doi.org/10.1016/j.electacta.2021.139581.
[6] H. Yao, Y. Song, Y. Chen, N. Wu, J. Xu, C. Sun, J. Zhang, T. Weng, Z. Zhang, Z. Wu, L. Cheng, D. Shi, X. Lu, J. Lei, M. Crispin, Y. Shi, L. Li, S. Li, Molecular architecture of the SARS-CoV-2 virus, Cell 183 (2020) 730–738.e13, https://doi.org/10.1016/j.cell.2020.09.018.
[7] S. Klein, M. Cortese, S.L. Winter, M. Wachsmuth-Melm, C.J. Neufeldt, B. Cerikan, M.L. Stanifer, S. Boulant, R. Bartenschlager, P. Chlanda, SARS-CoV-2 structure and replication characterized by in situ cryo-electron tomography, Nat. Commun. 11 (2020) 5885, https://doi.org/10.1038/s41467-020-19619-7.
[8] Z. Ke, J. Oton, K. Qu, M. Cortese, V. Zila, L. McKeane, T. Nakane, J. Zivanov, C. J. Neufeldt, B. Cerikan, J.M. Lu, J. Peukes, X. Xiong, H.-G. Kräusslich, S.H. W. Scheres, R. Bartenschlager, J.A.G. Briggs, Structures and distributions of SARS-CoV-2 spike proteins on intact virions, Nature 588 (2020) 498–502, https://doi.org/10.1038/s41586-020-2665-2.
[9] Z. Adamczyk, P. Batys, J. Barbasz, SARS-CoV-2 virion physicochemical characteristics pertinent to abiotic substrate attachment, Curr. Opin. Colloid Interface Sci. 55 (2021), 101466, https://doi.org/10.1016/j.cocis.2021.101466.
[10] A. Hohl, A.S. Ramms, C. Dohmen, K. Mantwill, A. Bielmeier, A. Kolk, A. Ruppert, R. Nawroth, P.S. Holm, Adenovirus particle quantification in cell lysates using light scattering, Hum. Gene Ther. Methods 28 (2017) 268–276, https://doi.org/10.1089/hgtb.2017.052.
[11] I. Makra, P. Terejánszky, R.E. Gyurcsányi, A method based on light scattering to estimate the concentration of virus particles without the need for virus particle standards, MethodsX 2 (2015) 91–99, https://doi.org/10.1016/j.mex.2015.02.003.
[12] P. Kramberger, M. Ciringer, A. Štrancar, M. Peterka, Evaluation of nanoparticle tracking analysis for total virus particle determination, Virol. J. 9 (2012) 265, https://doi.org/10.1186/1743-422X-9-265.
[13] Z. Szakács, T. Mészáros, M.I. de Jonge, R.E. Gyurcsányi, Selective counting and sizing of single virus particles using fluorescent aptamer-based nanoparticle tracking analysis, Nanoscale 10 (2018) 13942–13948, https://doi.org/10.1039/C8NR01310A.
[14] L. Yang, T. Yamamoto, Quantification of virus particles using nanopore-based resistive-pulse sensing techniques, Front. Microbiol. 7 (2016), https://doi.org/10.3389/fmicb.2016.01500.
[15] J.-L. Fraikin, T. Teesalu, C.M. McKenney, E. Ruoslahti, A.N. Cleland, A high-throughput label-free nanoparticle analyser, Nat. Nanotechnol. 6 (2011) 308–313, https://doi.org/10.1038/nnano.2011.24.
[16] E. van der Pol, F.A.W. Coumans, A.E. Grootemaat, C. Gardiner, I.L. Sargent, P. Harrison, A. Sturk, T.G. van Leeuwen, R. Nieuwland, Particle size distribution of exosomes and microvesicles determined by transmission electron microscopy, flow cytometry, nanoparticle tracking analysis, and resistive pulse sensing, J. Thromb. Haemost. 12 (2014) 1182–1192, https://doi.org/10.1111/jth.12602.
[17] Z. Varga, B. Fehér, D. Kitka, A. Wacha, A. Bóta, S. Berényi, V. Pipich, J.-L. Fraikin, Size measurement of extracellular vesicles and synthetic liposomes: the impact of the hydration shell and the protein corona, Colloids Surf. B Biointerfaces 192 (2020), 111053, https://doi.org/10.1016/j.colsurfb.2020.111053.
[18] B. Kiss, Z. Kis, B. Pályi, M.S.Z. Kellermayer, Topography, spike dynamics, and nanomechanics of individual native SARS-CoV-2 virions, Nano Lett. 21 (2021) 2675–2680, https://doi.org/10.1021/acs.nanolett.0c04465.
[19] A.C. Walls, Y.-J. Park, M.A. Tortorici, A. Wall, A.T. McGuire, D. Veesler, Structure, function, and antigenicity of the SARS-CoV-2 spike glycoprotein, Cell 181 (2020) 281–292.e6, https://doi.org/10.1016/j.cell.2020.02.058.
[20] N.R. Voss, M. Gerstein, 3V: cavity, channel and cleft volume calculator and extractor, Nucleic Acids Res. 38 (2010) W555–W562, https://doi.org/10.1093/nar/gkq395.